Structurally Enhanced Contrast in Photoacoustic Microscopy with F-Mode Imaging

Michael J. Moore, and Michael C. Kolios*
Department of Physics, Ryerson University
Institute for Biomedical Engineering, Science and Technology (iBEST), a partnership between Ryerson University and St. Michael's Hospital
Keenan Research Centre for Biomedical Science of St. Michael's Hospital
Toronto, Ontario, Canada
Email*: mkolios@ryerson.ca

***Abstract*—We present a new technique for photoacoustic (PA) image formation, termed 'F-Mode', which capitalizes on variations in the power spectrum of PA signals to produce images with object specific contrast. The technique is applied to a PA dataset by calculating the signal power spectrum at each scan location, segmenting it into discrete frequency bands, and then forming an image representing the spatial power distribution for each band. The appearance of differently sized objects in the resultant F-Mode images is dynamic, and is dictated by the presence of structure specific features in the power spectra. To demonstrate the technique, black polystyrene microspheres with diameters of 6 and 10 µm were scanned using a PA microscope equipped with a 400 MHz transducer and 532 nm laser. The images demonstrated that with appropriate selection of frequency band, visualization of either population of spheres could be selectively enhanced; the 6 µm spheres being more prominent at 249 MHz, while the 10 µm spheres dominated in the 425 MHz F-Mode image. Further, unique frequency dependent patterning in images of individual spheres pointed towards sub-micron diameter fluctuations in spheres from the same population. This proof-of-concept work paves the way for future *in vivo* applications, such as selectively analyzing blood vessels of different diameters.**

I. Introduction

In recent years, the use of Photoacoustic Microscopy (PAM) for the imaging of micron sized structures has rapidly increased [1]–[3]. The PAM technique leverages the intrinsic optical absorption of both organic (e.g. hemoglobin, DNA) [4], [5] and inorganic (e.g. dyes, nanoparticles, metals) [2] [6]–[8] materials to create striking images rich in contrast. Due to the short penetration depths required, transducers with central frequencies ranging from 20 – 80 MHz are typically utilized in PAM setups, as diffraction-limited lateral resolution is readily attainable through use of a tightly focused laser [3], [9].

The maximum amplitude projection (MAP) technique is the current gold standard for image formation in PAM. In MAP, images are formed by projecting the maximum amplitude of the RF-line acquired at each scan position onto a 2D grid. While the technique provides high-resolution lateral maps of optical absorption, it provides no detail in the depth dimension. Furthermore, this approach neglects the abundance of information encoded in the frequency domain of the broadband PA signals. For example, absorbers of different geometry and composition have unique spectral signatures in the frequency domain [10]–[13], which can be used for the assessment of the 3D structure of biological cells and stained organelles [14], [15].

In this work a new technique for PA image formation, termed 'F-Mode', is presented. The technique capitalizes on variations in the power spectrum of PA signals to produce images with object specific contrast not attainable in conventional MAP images. As a proof-of-concept, the F-Mode technique was used herein to selectively generate images of polystyrene microspheres of a specific diameter, and further, to visualize otherwise unresolvable sub-micron variation in the diameter of beads from the same population.

II. Theory

An illustration of the F-Mode algorithm is provided in Fig. 1. In this scenario, two spheres (shown as blue and red) of different radius are scanned with a PA microscope. First (Fig. 1i) each acquired RF line in the scan dataset is converted to its frequency domain representation via the Fast Fourier Transform (FFT), and the power spectra are computed. Next (Fig. 1ii), the spectrum is partitioned into K discrete frequency bands of equal length in a manner similar to that of [16]. The total power in each band is then calculated (Fig. 1iii), and stored in an array of size $K_{\times}m_{\times}n$. From this, K 'F-Mode' images of size $m_{\times}n$ can then be created (Fig. 1iv).

In an F-Mode image, pixels which capture minima in the summed power spectra will appear darker relative to the other pixels in the image. However, these same pixels may exhibit the highest summed power in a different frequency band, and thus will be the brightest pixels in the corresponding F-Mode images. The two bottom images in Fig. 1 demonstrate this inversion of contrast depending on frequency band used. In the F-Mode image generated from band denoted f_i, pixels corresponding to the larger sphere (blue power spectrum) have negligible total power compared to pixels from the smaller sphere (red power spectrum), due to the presence of a minimum in the blue power spectrum. The contrast between the two objects is reversed in band f_j, as now the red spectrum contains a minimum while the blue does not.

978-1-5386-3383-0/17/$31.00 ©2017 IEEE

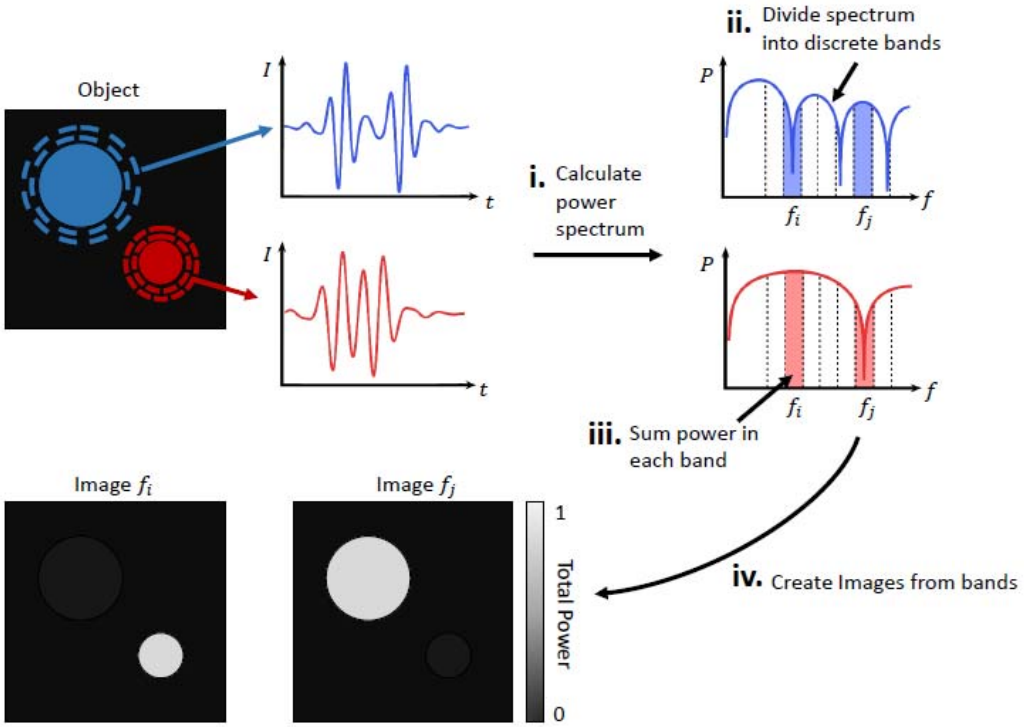

Fig 1: An overview of the F-Mode algorithm. PA signals are acquired from a large sphere (blue) and a small sphere (red). The power spectrum of each PA signal in the scan dataset is calculated, and partitioned into discrete frequency bands. The total power in each band at is computed at each scan position, and is used to form images

III. Methods

A. Sample Preparation

A 0.5% (w/v) solution of low melting point agarose (Sigma Aldrich, USA) dissolved in PBS was prepared. Approximately 300 µL of the molten agarose was pipetted into a glass bottom petri dish (MatTek, USA) and was allowed to solidify at room temperature for 30 minutes. In a separate aliquot, 2 µL of a stock PBS solution containing 6 µm black polystyrene microspheres (Polysciences, USA), and 2 µL of another PBS solution containing 10 µm black polystyrene microspheres (Polysciences, USA), was added to 1 mL of molten agarose. The aliquot was briefly vortexed before pipetting approximately 40 µL of the bead containing solution onto the top of the solidified agarose layer in the petri dish. The phantom was allowed to solidify at 4°C for 20 minutes prior to image acquisition.

B. Photoacoustic Measurement and F-Mode

A PA microscope (Kibero, Germany) equipped with a 532 nm laser (Teem Photonics, France) and 400 MHz transducer (Kibero, Germany) was used to raster scan the phantom [14]. The laser was focused using a 10X optical objective (Olympus, Japan), which was confocally aligned with the transducer on the opposing side of the sample. The laser and acoustic focal spots were approximately 2 µm and 4 µm, respectively. Acquired PA signals were sampled at a rate of 8 GHz using a 10-bit digitizer (Acqiris, USA), and were averaged 100 times to increase SNR. The FFT and power spectrum of the averaged RF-line acquired at each scan position was computed. The F-Mode algorithm outlined in the previous section was applied to the dataset with a band size of 2 MHz, and F-Mode images were generated for each spectral band.

IV. Results

A conventional MAP image of the phantom depicting three 6 µm spheres and one 10 µm sphere is shown in Fig. 2a. From this image a few salient observations can be made. First, the maximum PA intensity within each sphere in the image is comparable, regardless of size. This was expected as the spheres were provided by the same manufacturer and were of identical composition. Second, while the interior of the 6 µm spheres appeared to have uniform intensity, the 10 µm sphere had a prominent bright central region. Finally, there was no significant difference in the appearance of the size and shape of the 6 µm spheres as compared to one another.

A. F-Mode comparison of 10 µm and 6 µm spheres

Due to the similar PA intensities of both sizes of sphere, it is difficult to generate images depicting only spheres of a specific size with the MAP technique alone. However, due to the size dependent fluctuations in the power spectra, images of this type are readily created using the F-Mode technique. The F-Mode image created from the band centered at 249 MHz is shown in Fig. 2b). Here, the maximum intensity of the 10 µm sphere is less than 10% of the maximum intensity of the 6 µm sphere, and thus it is easily concealed by adjusting the lower bound of the dynamic range. This trend is reversed in the 425 MHz F-Mode image shown in Fig 2c)., where there is no

978-1-5386-3383-0/17/$31.00 ©2017 IEEE

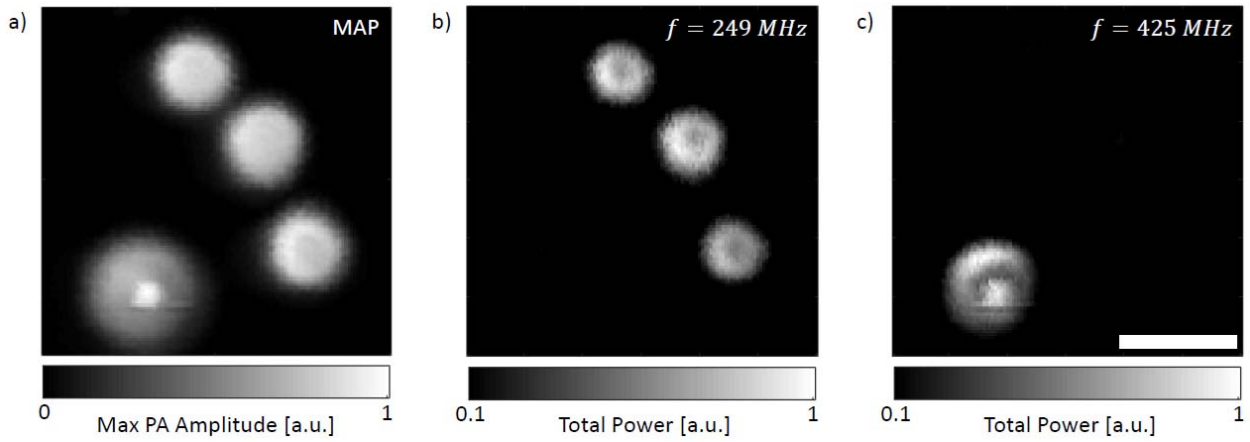

Fig. 2: a) MAP image depicting a single 10 µm microsphere and three smaller 6 µm spheres. F-Mode images showing only the 6 µm spheres (b) and 10 µm spheres (c) are formed using frequency bands centered at 249 MHz and 425 MHz, respectively. The scale bar is 10 µm, and applies to all images

indication of the 6 µm spheres, and only the 10 µm sphere is visible.

B. Comparison of the same object in different F-Mode images

The appearance of objects in the F-Mode technique is dynamic, and changes considerably with the selection of frequency band used for image generation. This is true not only when comparing the appearance of differently sized objects in the same frequency band (as in the previous section), but also when comparing the appearance of the same object in different frequency bands. To illustrate this, Fig. 3 shows how the appearance of F-Mode images of the 10 µm sphere evolve as a function of increasing frequency. The first band is centered at 201 MHz, with subsequent bands spaced 40 MHz apart to a maximum of 561 MHz. Several classifications of spatial power distribution are noted, for example: ring-like (241 MHz), bullseye (321 MHz), homogeneous (441 MHz), and point-like (561 MHz). Playing the entire F-Mode image stack as an animation allows for visualization of the transition between different appearances. While the physical basis behind these appearances has not yet been elucidated, it is hypothesized that they result due to inhomogeneous illumination of the microsphere and/or resonances which are created within the spheres. At each scan position only a fraction of the sphere is illuminated due to the tight optical focusing provided by the objective. This results in a variation in the optical excitation pattern as a function of scan position, which may in turn cause the measured spectra to deviate from those predicted for the case of homogeneous illumination [13]. Alternatively, resonances created in the microspheres can result in long PA time domain signals, akin to those produced in pulse-echo ultrasound [18], [19], and result in distinct spatial power distributions for particular resonant frequencies.

C. Detection of small variation in sphere size

Using the theoretical framework laid out in [14], it can be shown that a 10% increase in the radius of a liquid sphere results in a decrease of approximately 9% in the location of the observed spectral minima in the corresponding PA power spectrum. For this reason, the described F-Mode technique should be extremely sensitive to small deviations in absorber size and shape – provided the sharp minima in the power spectra are preserved, and that size of the spectral band is appropriately small.

Fig. 4 compares averaged F-Mode stair plots for each of the three 6 µm spheres shown in Fig 1a. The blue, orange, and yellow stair plots were generated by averaging 16 power spectra from the center of the top, middle, and bottom sphere, respectively. The stair plots show that each sphere attains a spectral minimum in a unique frequency band; all of which fall within a range of 16 MHz. The F-Mode image corresponding to the band containing the minimum for the bottom sphere (denoted with an arrow in Fig 4a) is shown in Fig 4b. In this image, the dynamic range has been dramatically reduced in order to visualize the 6 µm beads, which would otherwise be invisible due to the dominant 10 µm sphere. There is a marked difference in the appearance of the middle and bottom bead in this band. The bottom most bead has a ring-like appearance due to the presence of a spectral minimum, while the middle bead has transitioned away from its local minimum, and has attained a bulls-eye appearance. The top bead appears to be in a transitionary state between the ring-like and bulls-eye appearances. The different appearances of the spheres within this narrow frequency interval points towards sub-micron deviation in the sphere diameters. Furthermore, the similarity between these patterns and those observed in Fig. 3 for the 10 µm sphere, indicates the possibility of a deeper relationship between frequency band and spatial patterning. This relationship, as well as the minimum detectable change in sphere diameter, is currently the subject of further investigation.

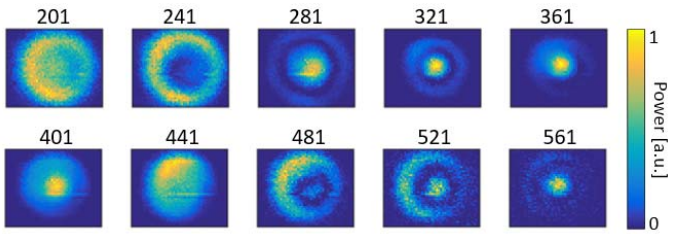

Fig. 3: F-Mode images of the same 10 µm microsphere formed from frequency bands spaced 40 MHz apart. The central frequency of each band, in MHz, is indicated above each image

978-1-5386-3383-0/17/$31.00 ©2017 IEEE

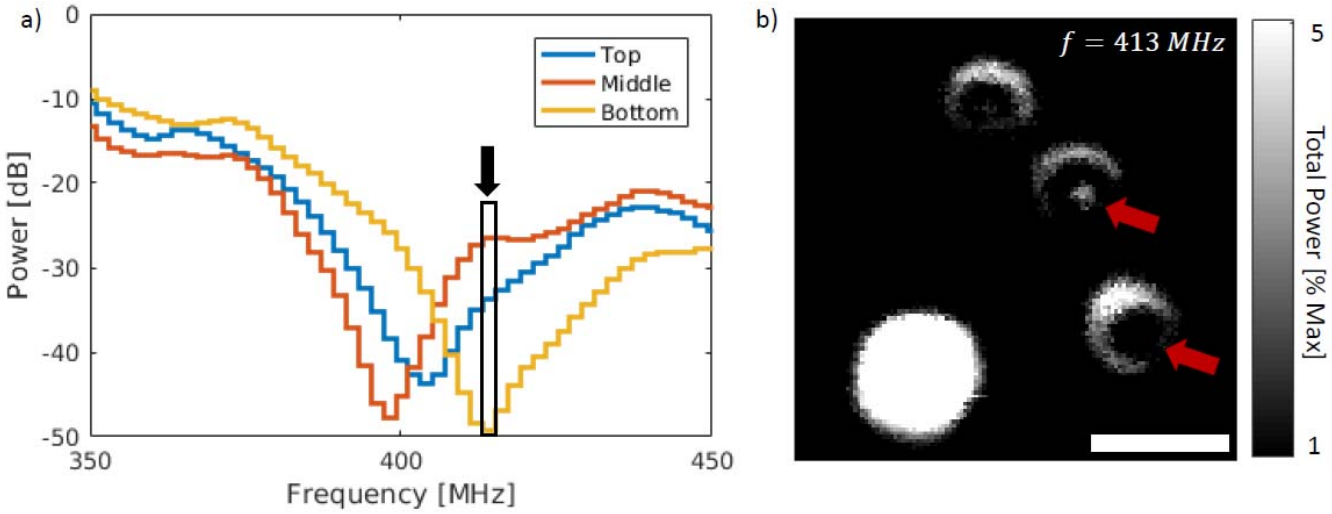

Fig. 4: **a)** Averaged F-Mode data from the 6 µm spheres shown in Fig 2a. Each sphere has a unique spectral minimum. **b)** F-Mode image formed from the band indicated with an arrow in a). The difference in the appearance of the middle and bottom spheres (denoted with arrows) is substantial, even though they have similar appearance in the MAP image

V. Discussion

A new technique for the display of PA images, termed 'F-Mode', was presented. The technique was applied to a conventionally acquired PA dataset to generate images with object specific contrast not attainable with the conventional MAP technique. F-Mode images of a single microsphere revealed a transition between several 'basis' appearances directly linked to the selected frequency band. Furthermore, it was shown that even slight differences in the summed power spectra are sufficient for the generation of substantially different F-Mode images. Future work will involve applying the technique in both *in vivo* and *ex vivo* biological models to selectively analyze blood vessels of different diameters, and investigating the applicability of the technique to PA datasets acquired with transducers with central frequencies ranging from pre-clinical (<40 MHz) to ultra-high (>1 GHz).

Acknowledgment

This research is supported in part by the Natural Sciences and Engineering Research Council of Canada, the Canadian Cancer Society, the Canadian Foundation for Innovation, the Ontario Ministry for Research and Innovation, and the Terry Fox Foundation.

References

[1] E. M. Strohm, M. J. Moore, and M. C. Kolios, "Single Cell Photoacoustic Microscopy: A Review," IEEE Journal on Selected Topics in Quantum Electronics, vol. 22, no. 3. 2016.

[2] E. M. Strohm, M. J. Moore, and M. C. Kolios, "High resolution ultrasound and photoacoustic imaging of single cells," Photoacoustics, vol. 4, no. 1, pp. 36–42, 2016.

[3] J. Yao and L. V. Wang, "Sensitivity of photoacoustic microscopy," Photoacoustics, vol. 2, no. 2, pp. 87–101, 2014.

[4] D.-K. Yao, K. Maslov, K. K. Shung, Q. Zhou, and L. V Wang, "In vivo label-free photoacoustic microscopy of cell nuclei by excitation of DNA and RNA.," Opt. Lett., vol. 35, no. 24, pp. 4139–4141, 2010.

[5] H.-C. Hsu, L. Wang, and L. V. Wang, "In vivo photoacoustic microscopy of human cuticle microvasculature with single-cell resolution," J. Biomed. Opt., vol. 21, no. 5, pp. 056004, 2016.

[6] L. D. Favro, P. K. Kuo, J. J. Pouch, and R. L. Thomas, "Photoacoustic microscopy of an integrated circuit," Appl. Phys. Lett., vol. 36, no. 12, pp. 953–954, 1980.

[7] S. Y. Zhang and L. Chen, "Photoacoustic Microscopy to Detect Subsurface Features of Integrated Circuits," Can. J. Phys., vol. 64, no. 9, pp. 1316–1319, 1986.

[8] J. R. Cook, W. Frey, and S. Emelianov, "Quantitative photoacoustic imaging of nanoparticles in cells and tissues," ACS Nano, vol. 7, no. 2, pp. 1272–1280, 2013.

[9] L. V. Wang, "Multiscale photoacoustic microscopy and computed tomography," Nat. Photonics, vol. 3, no. 9, pp. 503–509, 2009.

[10] G. J. Diebold, M. I. Khan, and S. M. Park, "Photoacoustic 'signatures' of particulate matter: optical production of acoustic monopole radiation.," Science, vol. 250, no. 4977, pp. 101–104, 1990.

[11] M. I. Khan, T. Sun, and G. J. Diebold, "Photoacoustic waves generated by absorption of laser radiation in optically thin cylinders," J. Acoust. Soc. Am., vol. 94, no. 2, pp. 931–940, 1993.

[12] E. Hysi, E. M. Strohm, and M. C. Kolios, "Probing Different Biological Length Scales Using Photoacoustics: From 1 To 1000 MHz," in Handbook of Photonics for Biomedical Engineering, A. H.-P. Ho, D. Kim, and M. G. Somekh, Eds. Springer Netherlands, 2014, pp. 1–18.

[13] M. I. Khan and G. J. Diebold, "The photoacoustic effect generated by an isotropic solid sphere," Ultrasonics, vol. 33, no. 4, pp. 265–9, 1995.

[14] M. J. Moore, E. M. Strohm, and M. C. Kolios, "Assessment of the Nucleus-to-Cytoplasmic Ratio in MCF-7 Cells Using Ultra-high Frequency Ultrasound and Photoacoustics," Int. J. Thermophys., vol. 37, no. 12, 2016.

[15] E. M. Strohm, E. S. L. Berndl, and M. C. Kolios, "Probing red blood cell morphology using high frequency photoacoustics," Biophys. J., vol. 105, no. 1, pp. 59–67, Jul. 2013.

[16] S. Tismer, S. Brand, S. Klengel, M. Petzold, and P. Czurratis, "Acoustic imaging of bump defects in flip-chip devices using split spectrum analysis," 2013 IEEE Int. Ultrason. Symp, pp. 950-3 (2013).

[17] R. E. Baddour, M. D. Sherar, J. W. Hunt, G. J. Czarnota, and M. C. Kolios, "High-frequency ultrasound scattering from microspheres and single cells," J. Acoust. Soc. Am., vol 117, no 2, pp. 934-943 (2005).

[18] O. Falou, A. Jafari Sojahrood, J. C. Kumaradas, and M. C. Kolios, "Surface modes and acoustic scattering of microspheres and ultrasound contrast agents," J. Acoust. Soc. Am., vol 132, no 3, pp. 1820-9 (2012).

978-1-5386-3383-0/17/$31.00 ©2017 IEEE